62 ~~17947~~ Copy 633

[redacted] NASA TM X-223

NASA TM X-223

Declassified by authority of NASA
Classification Change Notices No. 115
Dated ** 6/22/67

TECHNICAL MEMORANDUM

X-223 DECLASSIFIED-AUTHORITY-MEMO US:
2313. TAINE TO SHAUWLAS
DATED JUNE 15, 1967

PRESSURE MEASUREMENTS ON A HYPERSONIC GLIDE CONFIGURATION HAVING 79.5° SWEEPBACK AND 45° DIHEDRAL AT A MACH NUMBER OF 4.95

By Morton Cooper and Charles R. Gunn

Langley Research Center
Langley Field, Va.

GPO PRICE $ _____

CFSTI PRICE(S) $ _____

Hard copy (HC) 3.00

Microfiche (MF) .65

ff 653 July 65

FACILITY FORM 602

N67-31814 (ACCESSION NUMBER)

(THRU)

15 (PAGES)

1

TMX-223 (NASA CR OR TMX OR AD NUMBER)

01 (CATEGORY)

NATIONAL AERONAUTICS AND SPACE ADMINISTRATION

WASHINGTON November 1959

[redacted]

Declassified by authority of NASA
Classification Change Notices No. 113
Dated ** 6/28/67

[redacted]

NATIONAL AERONAUTICS AND SPACE ADMINISTRATION

TECHNICAL MEMORANDUM X-223

PRESSURE MEASUREMENTS ON A HYPERSONIC GLIDE CONFIGURATION HAVING 79.5° SWEEPBACK AND 45° DIHEDRAL AT A MACH NUMBER OF 4.95*

By Morton Cooper and Charles R. Gunn

SUMMARY

An experimental study of the pressures on a hypersonic glide configuration having 79.5° sweepback and 45° dihedral has been conducted in the Gas Dynamics Branch of the Langley Research Center at a Mach number of 4.95 and a Reynolds number of 15.7×10^6 based on body length. The angles of attack of the configuration referenced to the plane of the upper surface were 0°, 5°, and 10°. The pressures on the lower surface in the plane of symmetry approached the pressure that would exist on a swept infinite cylinder within a distance from the apex of about 7 nose diameters - the nose diameter in the plane of symmetry being used as the reference. Because of the low range of crossflow Mach numbers in the present investigation, 0.92 to 1.75, no adequate prediction of the pressures elsewhere could be made by either modified Newtonian or modified tangent-wedge approximations.

INTRODUCTION

An experimental program is now in progress in the Gas Dynamics Branch of the Langley Research Center to evaluate the effects of large dihedral on the aerodynamic characteristics of hypersonic glide configurations. The use of large dihedral was proposed in reference 1 as a means for alleviating the leading-edge heating problem on highly swept wings during hypersonic glide and reentry and a configuration having 79.5° planform sweepback and 45° dihedral was suggested as a means of fully exploiting the dihedral concept.

Low-speed stability tests of a very similar configuration (ref. 2) were encouraging as regards stability characteristics and maximum lift-drag ratio; however, the results indicated the need for further study to develop a suitable control arrangement.

*Title, Unclassified.

[redacted]

[redacted]

It is the purpose of the present paper to provide pressure data on this configuration at a Mach number of 4.95. The data are presented with limited analysis in order to expedite publication.

SYMBOLS

l	length of model (see fig. 1)
R_∞	free-stream Reynolds number, $\frac{\rho_\infty V_\infty l}{\mu_\infty}$
p	pressure
p_∞	free-stream pressure
p_r	pressure at ridge line
p_t	stagnation-point pressure behind normal shock
$p_{th,r}$	theoretical pressure at ridge line
$p_{t,\infty}$	free-stream stagnation pressure
r	radius of portion of cylinder generated by ridge line (see fig. 1)
$T_{t,\infty}$	free-stream stagnation temperature
V_∞	free-stream velocity
x	distance measured from apex, in plane of symmetry, along ridge line (see fig. 1)
x'	distance measured from apex, in plane of symmetry, along upper surface (see fig. 1)
y	distance around model from ridge line in plane perpendicular to ridge line (see fig. 1)
y'	distance from plane of symmetry along upper surface (see fig. 1)
α	angle of attack of model ridge line (see fig. 1)

L
6
0
4

[redacted]

α' angle of attack of plane of upper surface (see fig. 1)

μ_∞ free-stream viscosity

ρ_∞ free-stream density

Γ dihedral angle (see fig. 1)

Γ' local dihedral angle (see section B-B fig. 1)

L
6
0
4

APPARATUS, TESTS, AND METHODS

Jet

The tests were conducted in a 9-inch-diameter blowdown jet installed in the Gas Dynamics Branch of the Langley Research Center. The circular nozzle was designed by the method of characteristics and the ordinates were corrected for boundary-layer growth by assuming a turbulent boundary layer. The calibrated Mach number in the test section is approximately 4.95 with a maximum deviation from this nominal value of about 0.04 for a given pressure. The maximum running time of the jet for the stagnation conditions of the present investigation is in excess of 2 hours. Somewhat more detailed information is presented in reference 3.

Model and Instrumentation

The model was 6.5 inches long and was constructed from steel. The leading edges were swept back 79.5° in the plane of the upper surface; the dihedral was 45° in a plane perpendicular to the ridge line. A sketch of the pressure model is presented as figure 1 and a photograph, as figure 2. The sharp corners formed at the apex and formed at the intersections of the side planes and upper surface were rounded to approximately the radii indicated in figure 1. The ridge-line radius was constant for the entire body length.

The pressure orifices were 0.015 inch in diameter and the data were recorded either on mercury or butyl phthalate manometers, depending on the pressure range.

Installation

The support and actuating mechanism for inserting the model into the jet is shown in figure 3. In this figure, the model is shown

[redacted]

retracted from the jet. The model and its sting support were mounted to the side door assembly which, in turn, was attached to a pnuematic cylinder. The angle of attack was adjustable in a horizontal plane. The model was inserted into the proper testing position in the jet prior to flow initiation.

Test Conditions

All tests were conducted at a stagnation pressure of approximately 1,000 pounds per square inch and a stagnation temperature of 400° F. For these conditions, the Reynolds number based on a body length of 6.5 inches is 15.7×10^6. The specific stream conditions for each test are presented in table I. The angles of attack of the plane of the upper surface (α') were 0°, 5°, and 10°. The corresponding angles of attack of the ridge line were 10.7°, 15.7°, and 20.7°. L 6 0 4

Data Reduction

The pressure data obtained on the model have been nondimensionalized in terms of the free-stream stagnation pressure and are presented in table I. However, for purposes of analysis, the pressure data in figure 4 have been nondimensionalized in terms of the pressure on the stagnation line of an infinite cylinder[1] swept at the complement of the angle of attack α. This pressure, designated $p_{th,r}$, is simply the pressure that would be expected on the ridge line sufficiently far downstream from any apex effects. For reference purposes, the constants relating this pressure to stagnation pressure $p_{t,\infty}$, the stagnation-point pressure p_t, and the free-stream pressure p_∞ are

α', deg	$\frac{p_{th,r}}{p_{t,\infty}}$	$\frac{p_t}{p_{th,r}}$	$\frac{p_\infty}{p_{th,r}}$
0	0.00346	18.52	0.5785
5	.00569	11.25	.3516
10	.00889	7.21	.2251

[1]For $\alpha' = 5°$ and 10°, a shock exists parallel to the ridge line for the infinite cylinder because of the supersonic crossflow Mach number. No shock exists for $\alpha' = 0°$ because the crossflow Mach number is subsonic.

[redacted]

RESULTS AND DISCUSSION

The pressure distributions on the model are presented in figures 4 and 5 for angles of attack of the plane of the upper surface (α') of 0°, 5°, and 10°. The longitudinal pressure distributions in the plane of symmetry are presented in figure 4 for both the upper and the lower surface. Transverse pressure distributions are presented in figure 5 for two representative longitudinal stations (station A, $x/l = 0.40$; station B, $x/l = 0.80$). In all cases, upper-surface points have been flagged.

Longitudinal Distributions

The primary effect of the blunted nose of the configuration is to increase the pressure in the apex region. (See fig. 4.) The major part of this effect is restricted to less than 20 percent of the body length or about 7 nose diameters - the nose diameter (3/16 inch) in the plane of symmetry being used as the reference. The pressure on the ridge line downstream of this region rapidly approaches the value for the swept stagnation line.

As a matter of further interest, the ridge-line pressures downstream of the apex region have been compared with Newtonian theory which has been modified to the stagnation-point pressure - a procedure common for blunt bodies. These results, designated as Newtonian I in figure 4, were obtained from the following equation:

$$\frac{p - p_{\infty}}{p_t - p_{\infty}} = \sin^2\alpha \cos^2\Gamma'$$

or

$$\frac{p}{p_t} = \frac{p_{\infty}}{p_t} + \left(1 - \frac{p_{\infty}}{p_t}\right)\sin^2\alpha \cos^2\Gamma' \tag{1}$$

where p_{∞}/p_t is simply the ratio of the free-stream pressure to the stagnation-point pressure behind a normal shock for the test Mach number of 4.95. For the ridge, the local dihedral angle Γ' (fig. 1) is zero. The values of Newtonian I plotted in figure 4 are then

$$\frac{p}{p_{th,r}} = \frac{p}{p_t}\,\frac{p_t}{p_{th,r}}$$

[redacted]

where the second ratio on the right-hand side represents tabulated constants presented in the section entitled "Data Reduction."

Although the Newtonian theory gives a reasonable average prediction downstream of the apex region, it is clear that the swept-cylinder approximation is more definitive in that it is always a lower asymptote.

On the upper-surface center line (fig. 4), the asymptotic pressure is predicted surprisingly well by considering the upper surface as a two-dimensional expansion surface making an angle α' with respect to the free stream.

L
6
0
4

Transverse Distributions

The transverse pressure distributions (experimental pressure divided by experimental ridge-line pressure) on the lower surface have been compared with Newtonian I results, with a second modified Newtonian theory designated as Newtonian II, and with a modified tangent-wedge approximation. (See fig. 5.) The upper-surface pressures are compared with the same two-dimensional expansion pressure shown in figure 4.

In view of the agreement between the ridge-line pressure and the swept stagnation-line pressure in the vicinity of station A and station B, a modified Newtonian theory (Newtonian II) was calculated using the stagnation-line pressure on a swept infinite cylinder as a datum instead of the stagnation-point pressure. In order to be specific, the pressure at any transverse location y compared with the pressure at the ridge line is, for a fixed angle of attack, as follows:

$$\frac{p - p_\infty}{p_r - p_\infty} = \cos^2\Gamma'$$

or

$$\frac{p}{p_r} = \frac{p_\infty}{p_r} + \left(1 - \frac{p_\infty}{p_r}\right)\cos^2\Gamma' \tag{2}$$

The term p_∞/p_r is, in this particular approximation, interpreted as the ratio of the free-stream pressure to the stagnation-line pressure on a swept infinite cylinder; that is, $\frac{p_\infty}{p_r} = \frac{p_\infty}{p_{th,r}}$. (See section entitled "Data Reduction" for tabulated values.) The results from equation (2), designated as Newtonian II, are presented in figure 5. It is to be

[redacted]

noted that the Newtonian I curve is obtained by dividing the pressure distribution from equation (1) by the ridge-line value from equation (1).

The pressure in the modified tangent-wedge approximation was computed from the oblique-shock equation by utilizing the free-stream Mach number and the compression angle between the free-stream velocity vector and local planes tangent to the undersurface. This compression angle is $\sin^{-1}(\sin \alpha \cos \Gamma')$. These pressures were then nondimensionalized in terms of the ridge-line pressure (given by the tangent-wedge approximation) and the results are presented in figure 5. This procedure is similar to most applications of Newtonian theory which retain the form of the pressure distribution but discard the pressure level. The level is then established from a more reliable datum. For example, the known stagnation-point pressure is used as a reference datum in Newtonian I results and the stagnation-line pressure on a swept infinite cylinder is used in Newtonian II results. The actual pressure level given by the tangent-wedge approximation is exceedingly high in comparison with the present data.

A comparison of the lower-surface data with theoretical estimates (fig. 5) indicates wide discrepancies, a fact which is not very surprising since for $\alpha' = 0^\circ$ the Mach number normal to the ridge line (crossflow Mach number) is 0.92 and that for $\alpha' = 10^\circ$ is only 1.75. All the theoretical estimates are in close agreement with each other, particularly at the higher crossflow Mach numbers; hence, there is little preference between them.

The prediction of the upper-surface pressure is rather good for $\alpha' = 5^\circ$ and 10°.

CONCLUDING REMARKS

An experimental study of the pressures on a hypersonic glide configuration having 79.5° sweepback and 45° dihedral has been conducted in the Gas Dynamics Branch of the Langley Research Center at a Mach number of 4.95 and a Reynolds number of 15.7×10^6 based on body length. The angles of attack of the configuration referenced to the plane of the upper surface were 0°, 5°, and 10°. The pressures on the lower surface in the plane of symmetry approached the pressure that would exist on a swept infinite cylinder within a distance from the apex of about 7 nose diameters - the nose diameter in the plane of symmetry being used as the reference. Because of the low range of crossflow Mach numbers in

[redacted]

the present investigation, 0.92 to 1.75, no adequate prediction of the pressures elsewhere could be made by either modified Newtonian or modified tangent-wedge approximations.

Langley Research Center,
National Aeronautics and Space Administration,
Langley Field, Va., July 9, 1959.

L
6
0
4

REFERENCES

1. Cooper, Morton, and Stainback, P. Calvin: Influence of Large Positive Dihedral on Heat Transfer to Leading Edges of Highly Swept Wings at Very High Mach Numbers. NASA MEMO 3-7-59L, 1959.

2. Paulson, John W.: Low-Speed Static Stability and Control Characteristics of a Model of a Right Triangular Pyramid Reentry Configuration. NASA MEMO 4-11-59L, 1959.

3. Cooper, Morton, and Mayo, Edward E.: Measurements of Local Heat Transfer and Pressure on Six 2-Inch-Diameter Blunt Bodies at a Mach Number of 4.95 and at Reynolds Numbers Per Foot up to 81×10^6. NASA MEMO 1-3-59L, 1959.

[redacted]

L-604

TABLE I.- EXPERIMENTAL PRESSURE RATIOS $p/p_{t,\infty}$

	Values of $p/p_{t,\infty}$ for -		
	$p_{t,\infty}$ = 1,010 lb/sq in. $T_{t,\infty}$ = 400° F $R_\infty = 15.86 \times 10^6$ $\alpha' = 0°$	$p_{t,\infty}$ = 1,005 lb/sq in. $T_{t,\infty}$ = 400° F $R_\infty = 15.79 \times 10^6$ $\alpha' = 5°$	$p_{t,\infty}$ = 1,000 lb/sq in. $T_{t,\infty}$ = 420° F $R_\infty = 15.17 \times 10^6$ $\alpha' = 10°$
x/l	On ridge line		
0.05	6.072×10^{-3}	8.199×10^{-3}	11.364×10^{-3}
.10	4.849	7.003	10.267
.15	4.327	6.645	10.243
.20	4.052	6.475	9.950
.30	3.909	6.423	10.072
.40	3.798	6.345	9.901
.50	3.660	6.116	9.682
.60	4.092	6.022	8.804
x'/l	On upper-surface center line		
0.051	3.232×10^{-3}	2.316×10^{-3}	1.648×10^{-3}
.102	2.523	1.777	1.291
.153	2.109	1.469	1.084
.305	1.733	1.216	.934
.407	1.729	1.233	.934
.610	1.737	1.226	.938
.814	1.782	1.168	.791
y/r	Around body - station A		
0	3.798×10^{-3}	6.345×10^{-3}	9.901×10^{-3}
.598	3.418	5.125	7.537
.869	3.416	5.014	7.195
1.128	3.433	4.934	6.976
1.387	3.466	4.877	6.781
1.646	3.472	4.754	6.464
1.902	3.502	4.436	5.830
y'/r	On upper surface - station A		
0	1.729×10^{-3}	1.233×10^{-3}	0.934×10^{-3}
.487	1.762	1.183	.784
1.175	1.748	.505	.199
y/r	Around body - station B		
0	4.092×10^{-3}	6.022×10^{-3}	8.804×10^{-3}
.830	3.524	4.913	7.147
1.092	3.412	4.821	7.049
1.566	3.310	4.713	7.025
1.969	3.269	4.563	6.818
2.350	3.226	4.425	4.440
2.730	3.220	4.326	6.025
3.135	3.276	4.174	5.586
y'/r	On upper surface - station B		
0	1.782×10^{-3}	1.168×10^{-3}	0.791×10^{-3}
1.977	1.907	1.144	.533

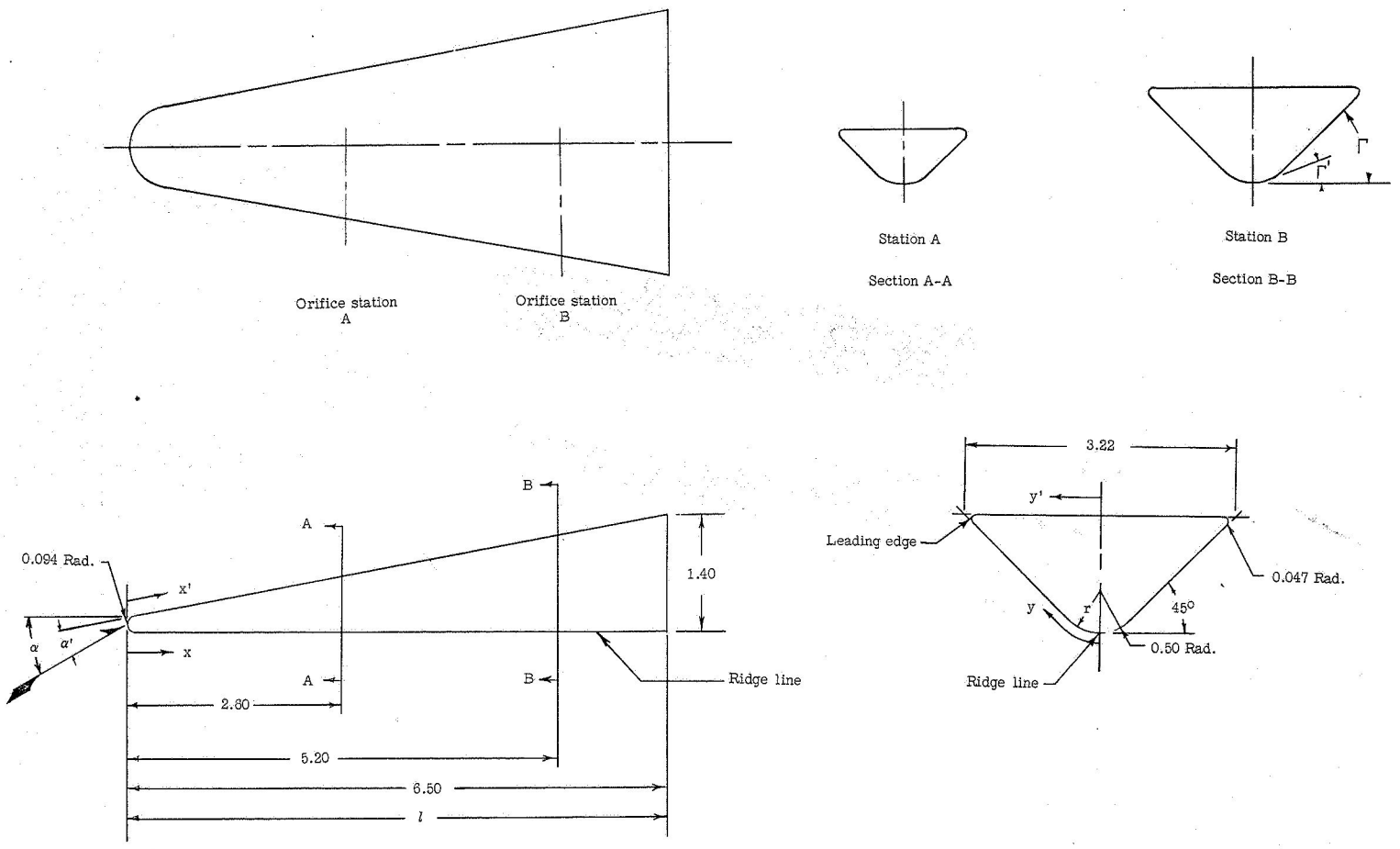

Figure 1.- Geometry of pressure model. Dimensions are in inches.

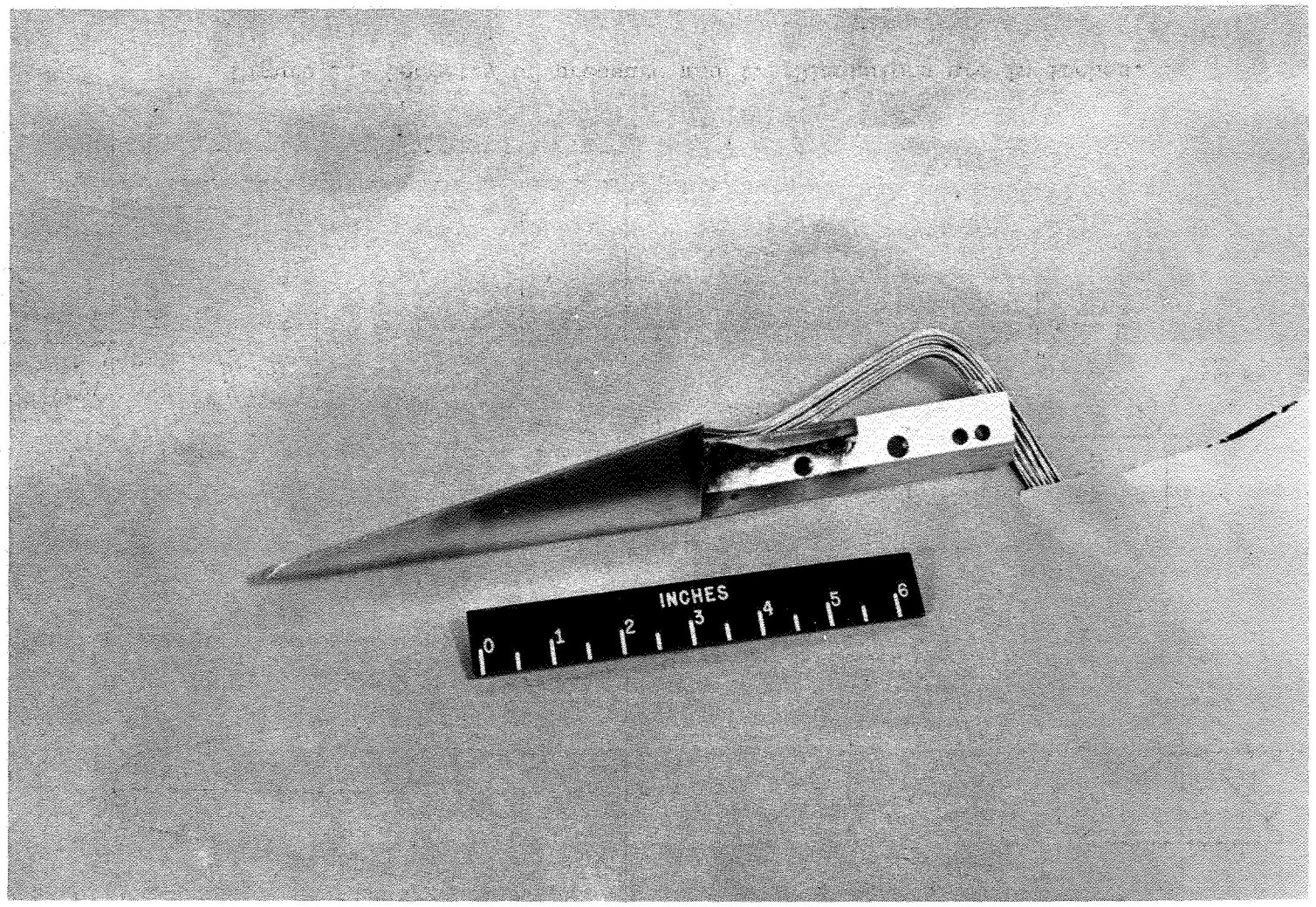

Figure 2.- Photograph of pressure model. L-59-1710

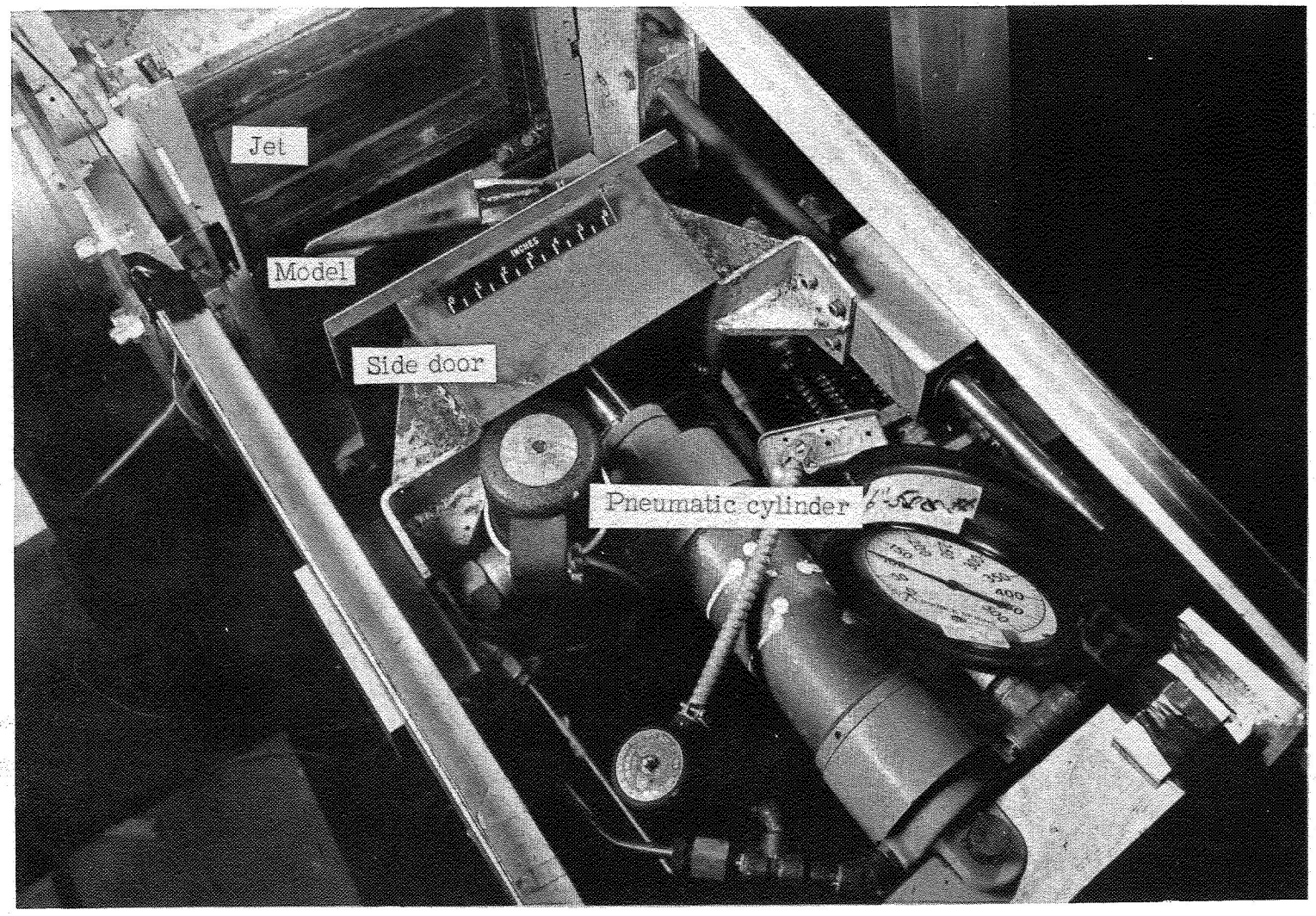

L-59-1709.1

Figure 3.- Model support and actuating mechanism for inserting model into the jet.

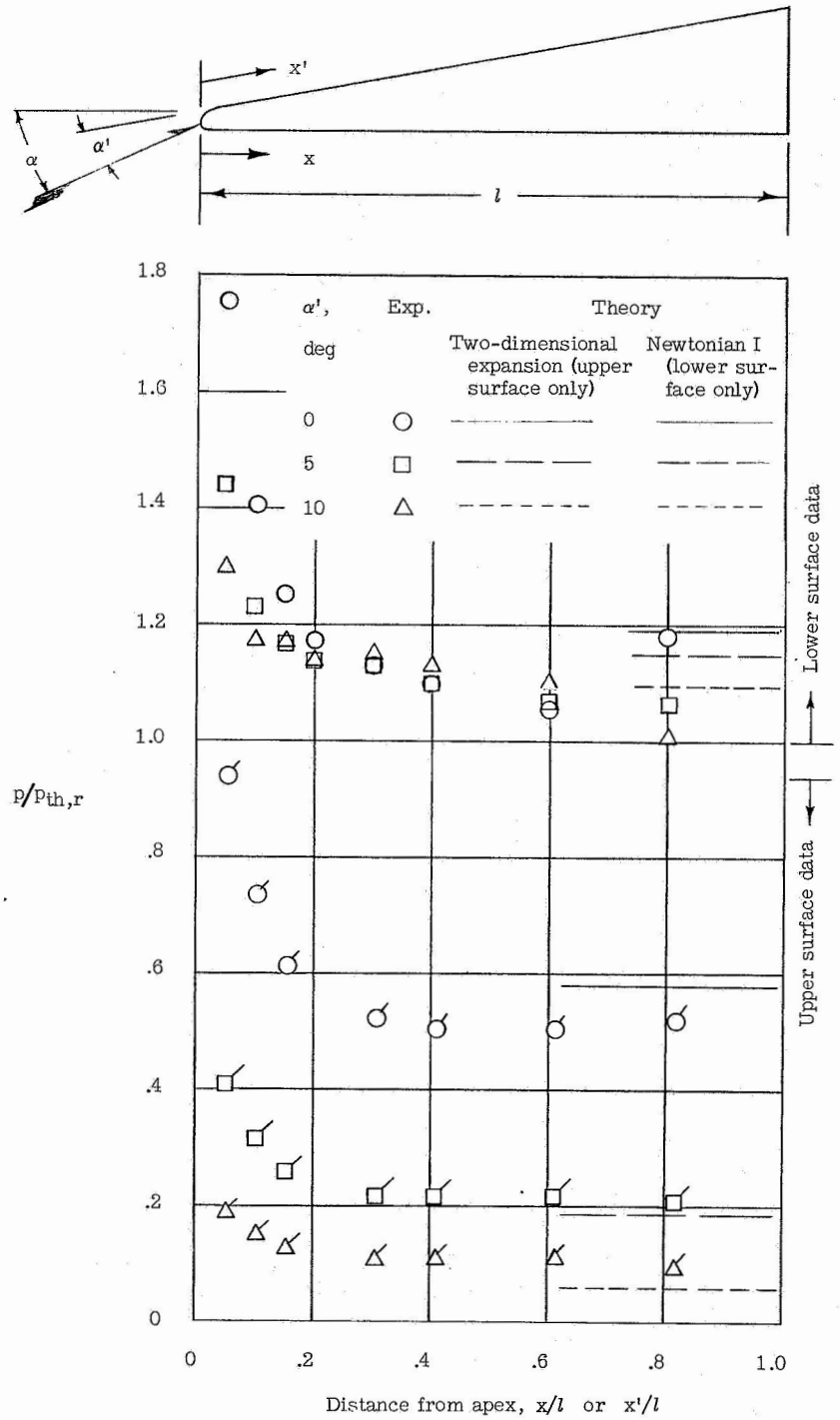

Figure 4.- Pressure distribution along ridge line and upper-surface center line. (Flagged symbols indicate upper-surface data and are plotted as a function of x'/l.)

[redacted]

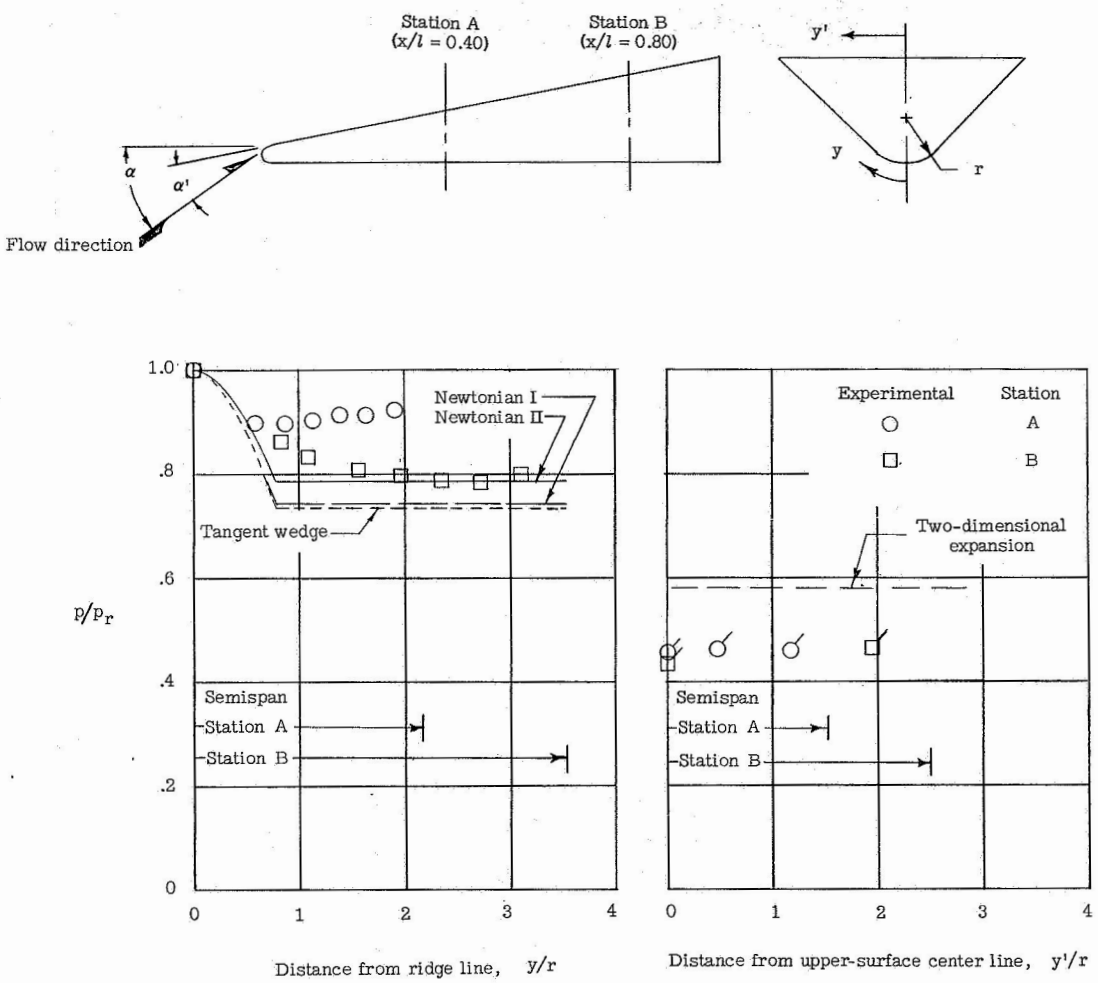

(a) $\alpha' = 0^{\circ}$.

Figure 5.- Pressure distribution around body at stations A and B. (Flagged symbols indicate upper-surface data and are plotted as a function of y'/r.)

L-604

[redacted]

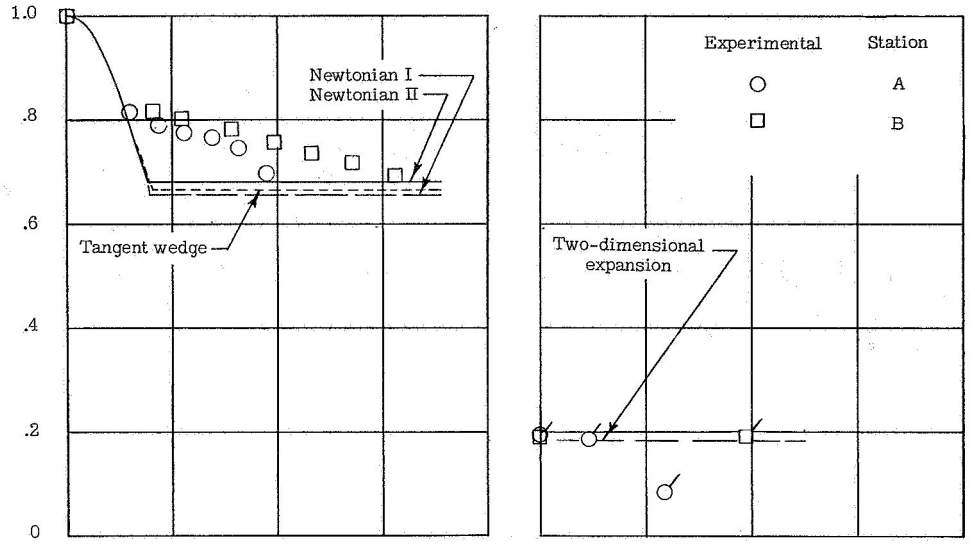

p/p_r

(b) $\alpha' = 5^{\circ}$.

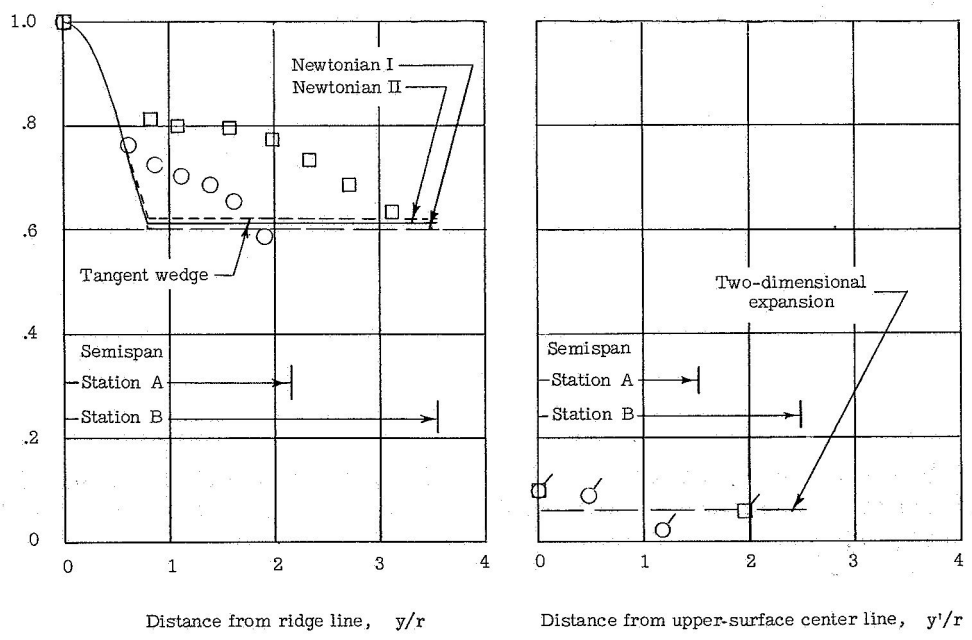

(c) $\alpha' = 10^{\circ}$.

Figure 5.- Concluded.